# MULTI-OBJECTIVE OPTIMIZATION OF HIGH-SPEED TRAIN INTEGRATED GROUNDING SYSTEMS USING NSGA-II

[1]CHAMUPANGWA SIINGWA, [2*]SONG XIAO, [3]ERNESTE NIBISHAKA, [4]YONGDONG HE, [5]HUI LI.

[1,2,3,4,5]School of Electrical Engineering, Southwest Jiaotong University, Chengdu 610031, China.
Email: [1]cham.siingwa@gmail.com, [2]xiaosong@home.swjtu.edu.cn, [3]enibishaka6@gmail.com,
[4]heyondon.swjtu@my.swtju.edu.cn, [5]3202828475@qq.com

**Abstract:** This study develops a multi-objective optimization framework for high-speed train integrated grounding systems, addressing the conflicting goals of minimizing train body (TB) current and transient overvoltage. Using a validated catenary–train–rail coupling model and the Non-dominated Sorting Genetic Algorithm II (NSGA-II), the study identifies Pareto-optimal grounding configurations that reduce TB current and overvoltage by up to 70% and 39%, respectively. The proposed framework eliminates manual tuning limitations and provides a systematic design tool for safer and more efficient grounding systems.

**Keywords**— High-speed train, integrated grounding system, train body overvoltage, multi-objective optimization, NSGA-II.

## 1. INTRODUCTION

The operational integrity of high-speed railways depends on a dynamic 'integrated grounding system' that provides a safe, low-impedance return path for traction current and ensures the safety of on-board low-voltage equipment and personnel [1][2]. This system combines protective grounding, which bonds exposed conductive parts to prevent electric shock, and working grounding, which serves as the return path for traction current from the train back to the substation.

The design of this system is not universal, leading to two primary on-board grounding schemes which are concentrated and distributed grounding scheme. In the concentrated scheme (Fig. 1a), protective grounding points are limited to a few carriages. In contrast, the distributed scheme (Fig. 1b), used in countries with ballastless tracks like China, installs grounding points at nearly every wheelset [2].

In the distributed scheme, both working grounding and protective grounding share the rail as a common discharge channel. The finite impedance of the rail creates a potential difference that drives a portion of the return current to divert from the rail back into the train body through a nearby protective grounding connection [3][4]. This circulating TB current is a known agent of electrochemical corrosion in wheel bearings and can damage sensitive on-board sensors and low-voltage control circuits [5].

Simultaneously, trains are vulnerable to overvoltage. These high-frequency, high-amplitude voltage surges are typically excited during routine but abrupt operational sequences, such as the raising of the pantograph or the closing of a vacuum circuit breaker (VCB) [6]. The resulting electromagnetic transients can couple into the train body, posing a severe risk of insulation failure in critical on-board equipment [7].

The engineering dilemma is thus clear: mitigation strategies for one problem often exacerbate the other. For instance, inserting resistance at protective grounding points can effectively block the path of TB current [8], but this same action increases the train body's impedance to ground, thereby amplifying transient overvoltage.

While previous research has proposed various solutions ranging from hybrid grounding schemes [8] to dedicated overvoltage suppressors [9], the design process for the distributed scheme, with its many variables, has remained largely iterative [10][11] and reliant on expert intuition.

Manual adjustment of grounding parameters is a time-consuming and sub-optimal approach, incapable of efficiently navigating the high-dimensional design space to find the best compromises. This paper addresses this design challenge by formulating the problem as a formal multi-objective optimization for a distributed grounding system. A high-fidelity 'catenary-train-rail' coupling model is developed and validated against experimental data to accurately simulate the system's behavior.

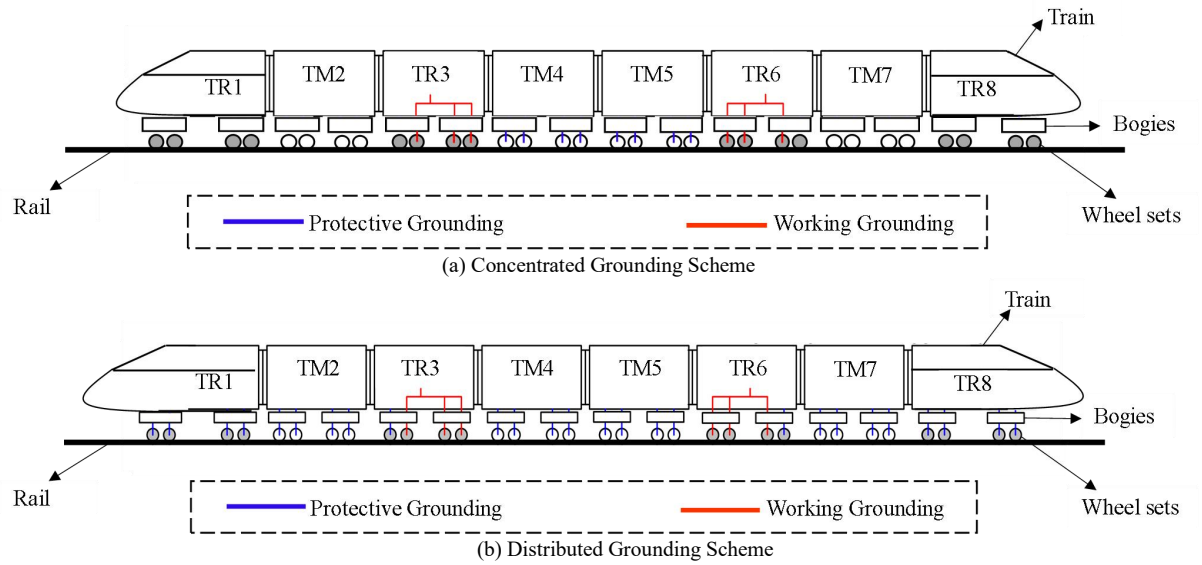


**Fig. 1. (a & b) Concentrated grounding scheme (Top) and distributed grounding scheme (Bottom)**

The core of the methodology in this paper is the application of the Non-dominated Sorting Genetic Algorithm II (NSGA-II). This algorithm is uniquely suited for this task, as it does not rely on pre-defined weightings of objectives [12]. Instead, it automatically discovers a Pareto-optimal set of solutions, each representing a different optimal trade-off between minimizing TB current and minimizing TB overvoltage.

This provides system designers with a clear, quantitative framework for selecting a grounding configuration that aligns with specific safety and performance priorities, moving the design process from empirical guesswork to a systematic and principled engineering discipline.

The remainder of this paper is structured as follows: Section II details the development and validation of the 'catenary-train-rail' coupling model. Section III introduces the NSGA-II algorithm and formulates the multi-objective optimization problem. Section IV presents and discusses the Pareto-optimal results and their performance improvements. Finally, Section V concludes the paper by summarizing the key findings and contributions.

## 2. THE 'CATENARY-TRAIN-RAIL' COUPLING GROUNDING MODEL AND ITS VALIDATION

This section details the development and validation of a high-fidelity 'rail–train' coupling model for an 8-unit train, essential for analyzing the trade-offs between train body (TB) current and overvoltage.

### 2.1. Model Architecture and Operating Principles

The model simulates key electrical interactions between the train and infrastructure, based on the direct power supply system common in China. As shown in Fig. 2(a), this system delivers 27.5 kV power via the catenary and provides a return path for traction current via the rail (dotted arrows).

The core model, depicted in Fig. 2, incorporates operational scenarios like pantograph raising/lowering and VCB switching. The catenary is modeled with an equivalent π-type circuit. Traction transformers in carriages TR3 and TR6 have their secondary-side loads simplified as equivalent resistances, with outputs connected to wheelsets for working grounding.

The model implements a distributed grounding scheme. Protective grounding points are installed at all wheelsets, not used for working grounding. A key feature differentiates trailer (TR) and motor (TM) carriages: TR carriages (TR1, TR3, TR6, TR8) use direct protective grounding, while TM carriages (TM2, TM4, TM5, TM7) include tunable resistors at their grounding points.

Due to the model's symmetry, the study focuses on carriages TR1, TM2, TR3, and TM4 to reduce computational complexity by 50% whilst attaining the same results. This setup defines the multi-variable design space for optimization, with the tunable resistors $R_{11}$, $R_{12}$, $R_{21}$, $R_{22}$, $R_3$, $R_{41}$, and $R_{42}$ (labeled in Fig. 2(b)) as the key parameters. The equivalent circuits of carriages TR and TM type is shown in Fig.2 (c(i)). The rail is segmented, with the impedance between any two points calculated based on its unit resistance and inductance as in Fig.2 (c(ii)).

Other parameters for the model are shown in Table 1.

**Table 1: Model Parameters**

| *Parameter* | *Value* | *Parameter* | value |
|---|---|---|---|
| $R_{11}$ | 25 mΩ | $L_{p3}$ | 3.6μH |

| *Parameter* | *Value* | *Parameter* | value |
|---|---|---|---|
| $R_{12}$ | 25 mΩ | $L_{p41}$ | 5.2μH |
| $R_{21}$ | 250 mΩ | $L_{p42}$ | 5.2μH |
| $R_{22}$ | 250 mΩ | $R_s$ | 0.165Ω |
| $R_3$ | 25 mΩ | $R_w$ | 4.45Ω |
| $R_{41}$ | 250 mΩ | $C_w$ | 0.1342μF |
| $R_{42}$ | 250 mΩ | $L_s$ | 10.8mH |
| $L_{p11}$ | 3.6μH | $L_w$ | 35.7mH |
| $L_{p12}$ | 3.6μH | ρR | 1.34Ω/Km |
| $L_{p21}$ | 5.2μH | ρL | 0.27mH/km |
| $L_{p22}$ | 5.2μH | | |

*ρR and ρL are resistance and inductance per kilometer for rail.

Transient TB overvoltage primarily originates from the high-voltage cable connecting the pantograph to the traction transformer. During switching events, a high-frequency surge is induced in the cable's shielding layer through the core-to-shield capacitance. The telegraph equations govern this propagation, which then transmits throughout the train body via the grounding system.

The telegraph equations are defined as:

$$\frac{\partial V}{\partial x} = -L\frac{\partial I}{\partial t} - RI \quad (1)$$

$$\frac{\partial I}{\partial x} = -C\frac{\partial V}{\partial t} - GV \quad (2)$$

Therefore, the high voltage cable can be modeled as a uniform transmission line as shown in Fig.2(c(iii)).

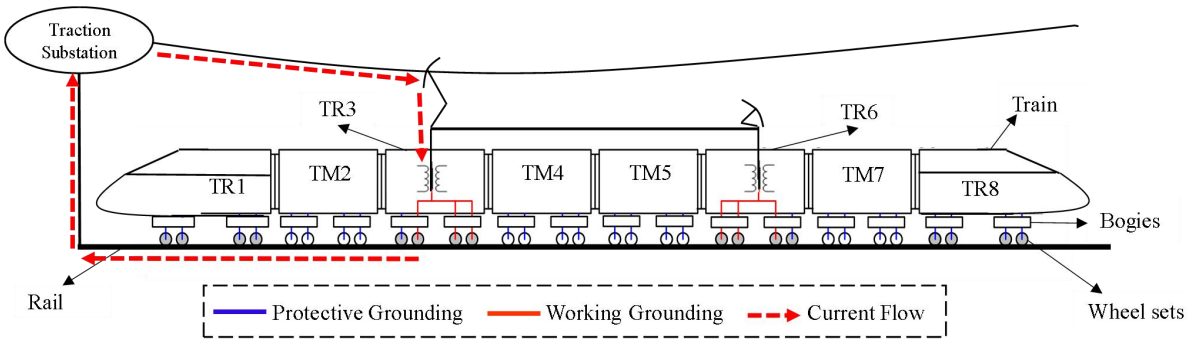


(a) The grounding scheme illustrating the location of working and protective grounding, and the path of current.

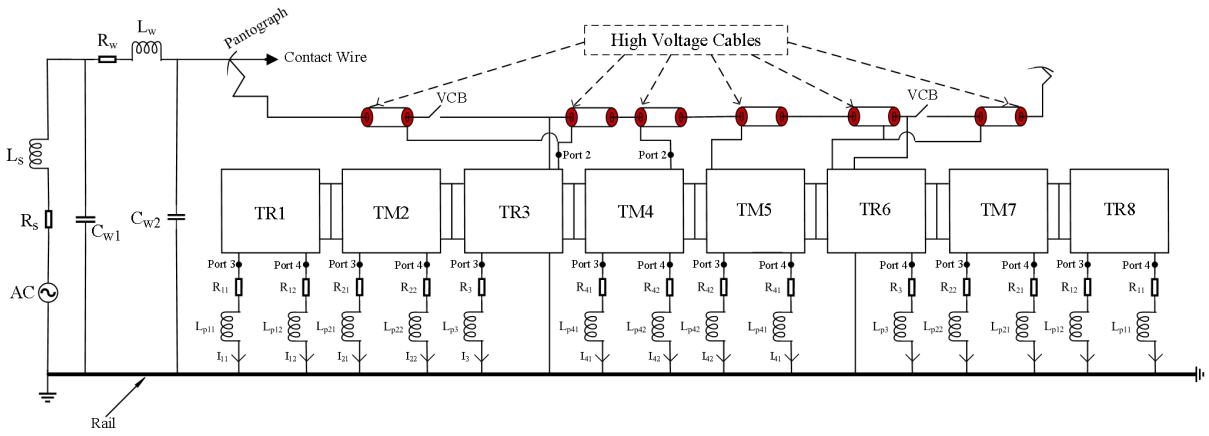


(b) Equivalent Circuit Model of traction Power supply and an eight (8) carriage train

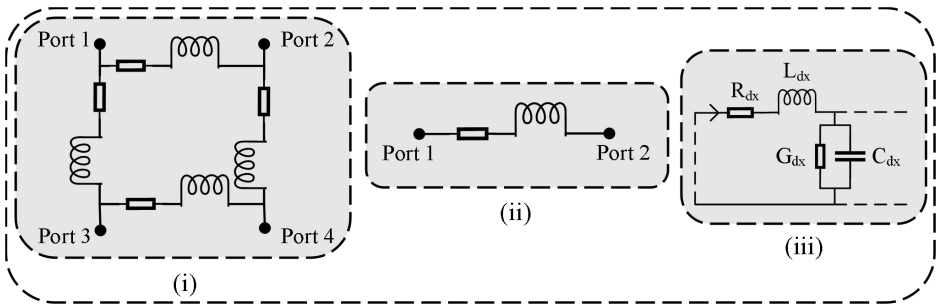


(c) The equivalent circuit models (i) TR and TM carriages, (ii) rail and (iii) high voltage cable.

**Fig. 2. (a, b & c). The 'Catenary-Train-Rail' coupling model**

## 2.2. Investigation and Validation of TB Overvoltage

The model was used to simulate two critical overvoltage scenarios: pantograph raising

and VCB switching. Experimental measurements were conducted on an actual train using voltage dividers connected between the train body and wheel axles. The maximum overvoltage that results from raising pantograph was recorded to be 3982 V while that of switching on the VCB was 8937 V. Compared with simulated results, errors were below 4% as shown in Table 1, and this confirmed the model's accuracy.

### 2.3. Safety Voltage Standard and Objective Definition

Following IEC/TS 60479-2 [13] and EN 50122-1 [14], the maximum safe overvoltage for a 0.4 ms surge is calculated to be 10,532.8 V. The measured overvoltage (up to ~9000V) is in a potentially hazardous zone to personnel and low-voltage on-board equipment. This establishes a clear and urgent objective: to minimize the TB overvoltage to reduce this inherent risk to personnel and to provide a greater safety margin for the on-board low-voltage equipment.

**Table 1: Experimental Compared to Simulated Maximum Train Body Overvoltage**

| *Parameter* | *Experimental Value* | *Simulation Value* | *Percentage Deviation* |
|---|---|---|---|
| Raising Pantograph | 3982 | 3867 | 3.80% |
| VCB Switching | 8937 | 8801 | 1.53% |

### 2.4 Investigation and Validation of TB Current

TB current arises from the current reflux between working and protective grounding points sharing the rail. Under dynamic conditions, current discharged from a working grounding point can flow back into the train body through a nearby protective grounding point.

To validate the model's prediction of TB current under both static and dynamic conditions, a comprehensive measurement campaign was undertaken. Initial tests were performed with the train stationary at a defined initial position.

Furthermore, to capture the complex transient behavior in a real-world scenario, measurements were specifically taken as the train passed through the neutral section, a dynamic condition that significantly perturbs the grounding system.

Experimental data was collected and then the effective (RMS) values of the TB current at various axles were calculated. The maximum was found to be 42.90 A as compared to the simulated value of 41.12 A as shown in Table 2.

**Table 2: Comparison of Experimental against Simulated RMS value of Train Body Current**

| *Parameter* | *Experimental Value* | *Simulation Value* | *Percentage Deviation* |
|---|---|---|---|
| TR1 Axle 1 | 42.90 | 41.12 | 4.15% |
| TR1 Axle 2 | 13.00 | 12.82 | 1.38% |
| TM2 Axle 2 | 1.04 | 1.01 | 2.88% |
| TM2 Axle 2 | 0.59 | 0.58 | 1.69% |
| TR3 | 35.00 | 33.56 | 4.11% |
| TR4 Axle 1 | 10.70 | 10.52 | 1.68% |
| TR4 Axle 2 | 8.60 | 8.26 | 3.95% |

The percentage deviations of simulated data from experimental data were less than 5%. The errors were attributed to simplifications in the model, such as neglecting certain parasitic capacitances.

The distribution and magnitude of this current, which can cause localized heating and interfere with sensors, defines our second objective which is to minimize the RMS TB current.

### 2.5. Summary of Optimization Objectives

Based on the model outputs and identified risks, the two core objectives are:

1. Minimize TB Overvoltage ($D_U$)
2. Minimize TB Current ($D_I$)

The subsequent section details the NSGA-II algorithm configuration for simultaneous optimization of these two conflicting objectives.

## 3. MULTI-OBJECTIVE OPTIMIZATION FRAMEWORK USING NSGA-II

The core design challenge for the integrated grounding system is a fundamental trade-off: minimizing Train Body (TB) overvoltage and TB current are conflicting objectives. This makes the problem inherently suited for multi-objective optimization.

Unlike weighted-sum methods which require pre-defined trade-offs and struggle with non-convex Pareto fronts, NSGA-II directly discovers a diverse set of Pareto-optimal solutions in a single run [15]. This provides a comprehensive map of the trade-off landscape, enabling an *a posteriori* decision-making process. A designer can select a final design from the Pareto front with a clear, quantitative understanding of the performance trade-offs.

### 3.1. Problem Formulation

The goal is to find the optimal set of grounding resistances that best balances the two competing objectives. The problem is formally defined as follows:

- Design Variables: The seven tunable protective grounding resistances in the model constitute the design vector, x:
  $\mathbf{x} = [R_{11}, R_{12}, R_{21}, R_{22}, R_3, R_{41}, R_{42}]$.

These variables are subject to lower and upper bounds ($0 \leq R_{ij} \leq 1$) for the integers $i$ and $j$ where $1 \leq i \leq 7$ and $1 \leq j \leq 7$.

- Objective 1: Minimize TB Overvoltage ($D_u$).
- Objective 2: Minimize TB Current ($D_i$).

The Multi-objective Optimization Problem is then stated as: Minimize $F(x) = [D_u(x), D_i(x)]$

Subject to: $x_{lb} \leq x \leq x_{ub}$

Where $x_{lb}$ is the lower bound and $x_{ub}$ is the upper bound in the design vector **x**.

### 3.2. The NSGA-II Algorithm

- Initialization: An initial population of candidate solutions (each a set of 7 resistances) is generated randomly within the specified bounds.
- Evaluation: Each candidate solution in the population is evaluated using the 'catenary-train-rail' coupling model to compute its objective function values, $D_u$ and $D_i$.
- Non-Crowding distance of each solution is computed to maintain diversity.
- Selection: A new parent population is created by selecting individuals from the combined parent and offspring populations based on rank and crowding distance.
- Genetic Operations: Simulated binary crossover and polynomial mutation are applied to create a new offspring population.
- Termination: All previous steps are repeated for a predetermined number of generations. The final output is the Pareto-optimal front.

## 4. RESULTS AND DISCUSSION

The NSGA-II algorithm was implemented with the parameters specified in Table 3 to optimize the integrated grounding system.

**Table 3: NSGA-II Parameters**

| *Parameter* | *Value* |
|---|---|
| Population size | 100 |
| Maximum Generations | 200 |
| Crossover Fraction | 0.8 |
| Number of Variables | 7 |
| Mutation Rate | 0.05 |
| Resistance Range | 0.01-1.00Ω |
| Selection Method | Non-dominated Sorting |

Population size and generations were chosen to explore the complex 7D resistance space. Crossover and mutation rates balanced solution refinement with diversity preservation. Non-dominated sorting was employed to maintain the Pareto-optimal front throughout the optimization process. The outcome of this shown in the Fig.3.

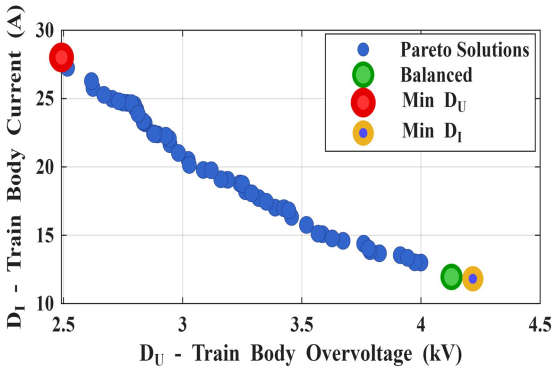


**Fig. 3. The Pareto front showing optimal trade-off**

The algorithm converged after 150 generations with 45 minutes computational time.

### 4.1 The Pareto-Optimal Front and Trade-off Analysis

In Fig.3, each point represents a unique, optimal set of grounding resistances, illustrating the fundamental conflict between the two objectives: achieving a very low TB current results in a high overvoltage, and vice-versa.

The maximum overvoltage and current for the manual case and the balanced optimized case where compared and results are shown in table 4.

**Table 4: Comparison of the manual (Original) scheme against Balanced optimized scheme**

| *Parameter* | *Manual Scheme* | *Optimized Scheme* | *Percentage Reduction* |
|---|---|---|---|
| Maximum Train body Current | 42.90 A | 12.69 A | 70% |
| Maximum overvoltage | 6.460 kV | 3.930 kV | 39% |

The optimized balanced Solution achieves a 39**%** reduction in maximum average overvoltage, which results from VCB switching overvoltage and pantograph raising, and a 70% reduction in maximum RMS TB current compared to the original design. This simultaneous improvement in both conflicting objectives highlights the value of a systematic optimization approach over manual tuning.

### 4.2 Performance of Selected Optimal Solutions

To demonstrate practical utility, three representative solutions from the Pareto front were selected for analysis, as illustrated in Fig. 4.

Solution A (Current-Optimized): Minimizes TB current at the cost of higher overvoltage.

Solution B (Balanced): A compromise from the 'knee' region of the front.

Solution C (Overvoltage-Optimized): Minimizes TB overvoltage while accepting a higher current.

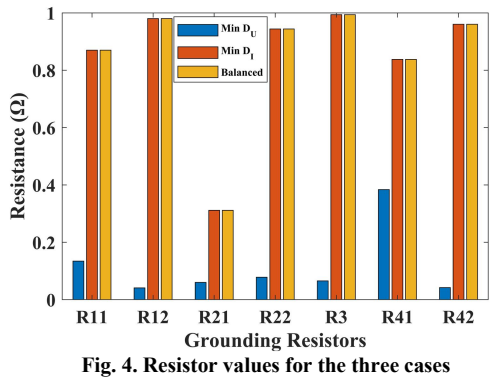


**Fig. 4. Resistor values for the three cases**

**Fig.4. Resistor values for the three cases**

The variation in these values across the front reveals the complex, non-intuitive relationships between individual grounding points and the system-level objectives, which would be exceedingly difficult to discover manually.

Additionally, analysis revealed that R3, positioned at the transformer-car grounding interface, exerts dominant influence on system performance due to its strategic location in both the primary traction current path and the body overvoltage coupling network. Its influence on both train body overvoltage and current is shown in Fig.5.

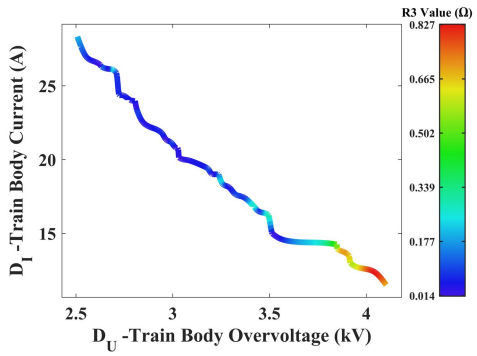


**Fig. 5. The Pareto front showing optimal trade-off**

This makes R3 the most effective control parameter for engineering the overvoltage-current trade-off.

## 5. CONCLUSION

This paper has developed a high-fidelity 'rail-train' coupling model, which was rigorously validated against experimental data, demonstrating its accuracy in simulating both TB current under dynamic conditions and high-frequency overvoltage during transient events like pantograph raising and VCB switching. This model then served as the foundation for the optimization process.

The paper ended with addressing the critical design challenge of balancing train body (TB) current and transient overvoltage in the integrated grounding system of high-speed trains. Moving beyond conventional single-objective or weighted-sum optimization approaches. The problem was formulated and solved using a robust multi-objective framework centered on Non-dominated Sorting Genetic Algorithm II.

## ACKNOWLEDGMENTS

The author gratefully acknowledges the financial support provided by the Ministry of Commerce of the People's Republic of China (MOFCOM) Scholarship, which enabled the completion of this research. Special thanks are extended to Professor Xiao Song for his invaluable guidance, insightful supervision, and constructive feedback throughout the study.

## REFERENCES

[1] L. Wei, L. Lingyun, M. Qingan, L. Xuefei and A. Ahmed Bhatti, "Vehicle-Ground United Traction Power Supply Calculation in Dual-System Train Grounding System," *J. Southwest Jiaotong Univ.*, vol. 59, no. 3, pp. 501-509, 2024, doi: 10.3969/j.issn.0258-2724.20220655.

[2] G. Wu, G. Gao, and J. K. Sykulski, "3-D modelling of an integrated grounding system for high-speed trains considering rail–train current reflux," in *Proc. Int. Conf. on Railway Electrical Systems*, 2021. [Online]. Available: ResearchGate.

[3] A. A. Bhatti, B. He, and X. Wang, "Analysis of rail potential and stray current with a unified traction power system model," *Railway Engineering Science*, Springer, 2024. [Online]. Available: SpringerLink.

[4] S. Yang, "Discrete modeling and calculation of traction return-current network concerning impedance equivalent," *Journal of Electrical and Mechanical Engineering*, 2023. [Online]. Available: SAGE Journals.

[5] E. Nibishaka, S. Xiao, T. Zhu, Y. Cao, T. Li, and G. Wu, "Analysis of Electrochemical Corrosion in Traction Motor's Bearings Considering Overvoltage and Stray Current in High-Speed Trains," *Journal of Information Systems Engineering and Management*, vol. 10, no. 34s, Apr. 12 2025. DOI: 10.52783/jisem.v10i34s.5825.

[6] D. Jiang, H. Zou, Y. Guo, F. Tian, H. Liu, and Y. Yin, "Simulation on operating overvoltage of dropping pantograph based on pantograph–catenary arc and variable capacitance model," *Applied Sciences*, vol. 14, no. 16, art. 6861, 2024. DOI: 10.3390/app14166861. [Online]. Available: MDPI.

[7] Y. Guo *et al.*, "Research on ultra-fast transient overvoltage characteristics of electric locomotive," *Applied Sciences*, 2024. [Online]. Available: MDPI.

[8] K. Vranešić, "Measures and prescriptions to reduce stray current in the design of new track corridors," *Energies*, 2023.

[9] U. Kornkanok, S. Deeon, and S. Wongcharoen, "Applications of safety transient voltage suppressors in the track circuits of railway signaling systems," *EUREKA: Physics and Engineering*, no. 1, pp. 47–58, 2024. doi: 10.21303/2461-4262.2024.003074. [Online]. Available: https://doi.org/10.21303/2461-4262.2024.003074.

[10] K. Ziba and S. Xiao, "Impact analysis of high-speed train grounding modes on the magnetic distribution of train bodies," presented at/available online, Jun. 19, 2024.

[11] S. Xiao, M. Tong, Y. Li, Z. Ye, D. Zhai, Y. Jin, H. Hou, Y. Shen, J. Zhou, J. Liu, J. Wu and Y. Rao, "The performance analysis of the 'train-rail' grounding system for high-speed trains considering circumflux and train body voltage,"

*IEEE Transactions on Vehicular Technology*, vol. 70, no. 10, pp. 9957-9971, Oct. 2021. doi: 10.1109/TVT.2021.3109916.

[12] Z. Zhang, "Pareto multi-objective optimization of metro train energy using improved NSGA-II," *Computers & Electrical Engineering*, 2023. [Online]. Available: ScienceDirect.

[13] *IEC/TS 60479-2:2019*, *Effects of current on human beings and livestock — Part 2: Special aspects*. International Electrotechnical Commission, 2019. [Online]. Available: webstore.iec.ch.

[14] *EN 50122-1:2022*, *Railway applications — Fixed installations — Electrical safety, earthing and the return circuit — Part 1: Protective provisions against electric shock*. CENELEC, 2022. [Online]. Available: iTeh Standards

[15] S. Xing, K. Li, L. Zhang *et al.*, "Robust optimization of energy-saving train trajectories under passenger load uncertainty based on p-NSGA-II," *IEEE Transactions on Transportation Electrification*, 2023 / 2024. [Online]. Available: ScienceDirect